Draft version September 4, 2025
Typeset using LaTeX twocolumn style in AASTeX631

Kilonovae and Long-duration Gamma-ray Bursts

Marko Ristić,[1,2,*] Brandon L. Barker,[2,3,†] Samuel Cupp,[1,2] Axel Gross,[1,2] Nicole Lloyd-Ronning,[2,3] Oleg Korobkin,[1,2] Jonah M. Miller,[2,3,4] and Matthew R. Mumpower[1,2]

[1] *Theoretical Division, Los Alamos National Laboratory, Los Alamos, NM 87545, USA*
[2] *Center for Theoretical Astrophysics, Los Alamos National Laboratory, Los Alamos, NM 87545, USA*
[3] *Computational Division, Los Alamos National Laboratory, Los Alamos, NM 87545, USA*
[4] *Michigan SPARC, Los Alamos National Laboratory, Ann Arbor, MI 48105, USA*

(Dated: September 4, 2025)

ABSTRACT

Recent detections of kilonova-like emission following long-duration gamma-ray bursts GRB211211A and GRB230307A have been interpreted as originating from the merger of two neutron stars. In this work, we demonstrate that these observations are also consistent with nucleosynthesis originating from a collapsar scenario. Our model accurately predicts the observed optical and infrared light curves using a single weak r-process component. The absence of lanthanide-rich material in our model, consistent with the data, challenges the prevailing interpretation that a red evolution in such transients necessarily indicates the presence of heavy r-process elements.

Keywords: Core-collapse supernovae (304), Gamma-ray bursts (629), Nuclear astrophysics (1129), Nucleosynthesis (1131), R-process (1324)

1. INTRODUCTION

For over three decades, it has been known that the gamma ray burst (GRB) duration distribution is bimodally split, with so-called "short" GRBs lasting $\lesssim 2$ seconds, and "long" GRBs lasting $\gtrsim 2$ seconds (Kouveliotou et al. 1993). Long GRBs have been tied to the collapse of massive star progenitors (collapsars) through, among other arguments, observations of coincident supernova in their light curves and spectra (Galama et al. 1998; Hjorth et al. 2003; Woosley & Bloom 2006; Hjorth & Bloom 2012) as well as their locations in star forming regions in their host galaxies (Bloom et al. 2002; Fong et al. 2010; Fong & Berger 2013; Lyman et al. 2017). The progenitors of short GRBs were postulated to be compact object mergers (double neutron star, or neutron star-black hole) and this was put on firm footing with coincident multimessenger detection of a short-GRB and gravitational waves from a neutron star merger (The LIGO Scientific Collaboration et al. 2017a,b).

Recently, however, a handful of long GRBs have been categorized as originating from compact object mergers. Two notable examples include GRB 211211A (Rastinejad et al. 2022) and GRB 230307A (Yang et al. 2024; Levan et al. 2024), with prompt durations lasting about 40 seconds in each case. In determining the progenitors of these GRBs, these studies present the presence of late-time infrared emission as a key signature indicating heavy-element nucleosynthesis stemming from a compact object merger. Additionally, Levan et al. (2024) present JWST spectra of GRB230327A at 29 and 61 days, showing evidence of an emission line at 2.15 microns which they interpret as Te III. The spectra also suggest the potential presence of W III and Se III at these later times. These interpretations suggests heavy element production at the site of a long GRB.

Previous discussions of long GRBs with kilonova signatures have all assumed a binary neutron star merger progenitor for these events, with nucleosynthesis occurring from the extant neutron-rich environment of a tidally disrupted neutron star (Rastinejad et al. 2022;

mristic@lanl.gov

* ISTI Fellow
† Metropolis Fellow

Yang et al. 2024; Troja et al. 2022; Yang et al. 2022; Zhang et al. 2022; Levan et al. 2024; Sun et al. 2025; Gottlieb et al. 2025). Although recent studies have shown (e.g. Gottlieb et al. 2025) that compact object mergers can make GRBs on the order of 10's of seconds, there exists an unavoidable basic limitation of a compact object merger in powering a GRB, at least in the case of a black hole-disk central engine: the duration, τ, of the prompt gamma-ray emission. This duration (which is roughly set by the lifetime of the jet[1], for cases where the prompt emission arises from internal dissipation processes in the jet) is determined by the amount of material available in the disk (M_{disk}) divided by the accretion rate ($\dot{M}$) of this material onto the central engine: $\tau \sim M_{disk}/\dot{M}$.

Galactic chemical evolution studies have also shown the presence of heavy element production very early in the history of our galaxy (e.g. Côté et al. 2019, and references therein). A recent study by Saleem et al. (2025) showed that even when allowing for the shortest possible merger delay-time distributions in binary neutron star and neutron star-black hole mergers, these compact binary mergers alone cannot account for the observed heavy metal enrichment in metal poor stars in our galaxy.

Additionally and compellingly, when GRB211211A and GRB230307A are analyzed in a detailed high-dimensional parameter space (Negro et al. 2025) — accounting for both spectral and fine-scale temporal information over the duration of the burst — both of these GRBs appear to align with the phase space populated by GRBs associated with collapsars[2] (i.e. the region where those GRBs that have an observed coincident supernova fall; see Figure 2 and the Appendices of Negro et al. 2025).

The collapsar system (Woosley 1993; MacFadyen & Woosley 1999a) is a collapsing massive star that produces a rapidly rotating black hole-accretion disk central engine that launches a relativistic outflow through the so-called Blandford-Znajek process (Blandford & Znajek 1977; MacDonald & Thorne 1982). In this process, rotation and frame-dragging effects near the black hole horizon cause a build-up of Poynting flux along the spin axis of the black hole. The powerful jet can carry enough energy and momentum to punch through the surrounding stellar material and propagate into the circumstellar medium where it is inferred from observations to have Lorentz factors on the order of hundreds to thousands (see, e.g., Ghirlanda et al. 2018, and references therein). As the jet is launched from the central engine and traverses the in-falling stellar material, a so-called "cocoon" region is created - a hot, dense region surrounding the jet, but with smaller outflow velocity (Ramirez-Ruiz et al. 2002; Bromberg et al. 2011, 2014).

[1] More precisely, the observed duration is the timescale over which the engine operates after the jet breaks out of the star, as in equation 2 of Bromberg et al. (2012).

[2] See also Barnes & Metzger (2023)

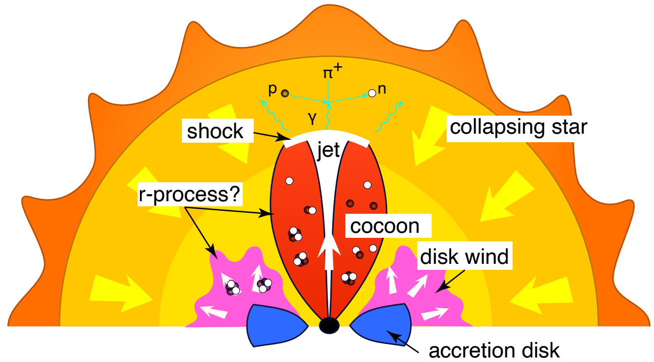

Figure 1. Schematic of a collapsar showing the two proposed sites for neutron-rich nucleosynthesis, emanating from the jet/cocoon or from the disk wind.

Mumpower et al. (2025) have recently proposed a new process and site for the production of heavy elements: the complex interaction of light and matter within a relativistic GRB jet stemming from a collapsar. Mumpower et al. (2025) showed that as the jet is crossing the dense stellar material, if the flux of high energy photons is sufficient, photons will interact with the shock compressed material at the jet head and high-energy, photohadronic interactions may lead to an excess of neutron production at the jet head. These neutrons then propagate into the hot, dense cocoon region, allowing for rapid neutron capture process (r-process) nucleosynthesis.

In this paper, we show how this model of nucleosynthesis in this collapsar scenario can reproduce the observations of kilonovae in GRBs 211211A and 230307A. Our paper is organized as follows: in Section 2, we describe the methods we use to compute the predicted r-process signatures around the jet head, both under some basic assumptions without prior knowledge of the observations and with a more thorough Bayesian inference analysis. In Sections 3 and 4, we show how these light curves reproduce the observed data remarkably well and present discussion of the implications of these results. Finally, in Section 5, we present our conclusions.

2. METHODS

2.1. *Nucleosynthesis Calculations*

In the standard picture of collapsars, nucleosynthesis originates in winds that arise after the creation of an ac-

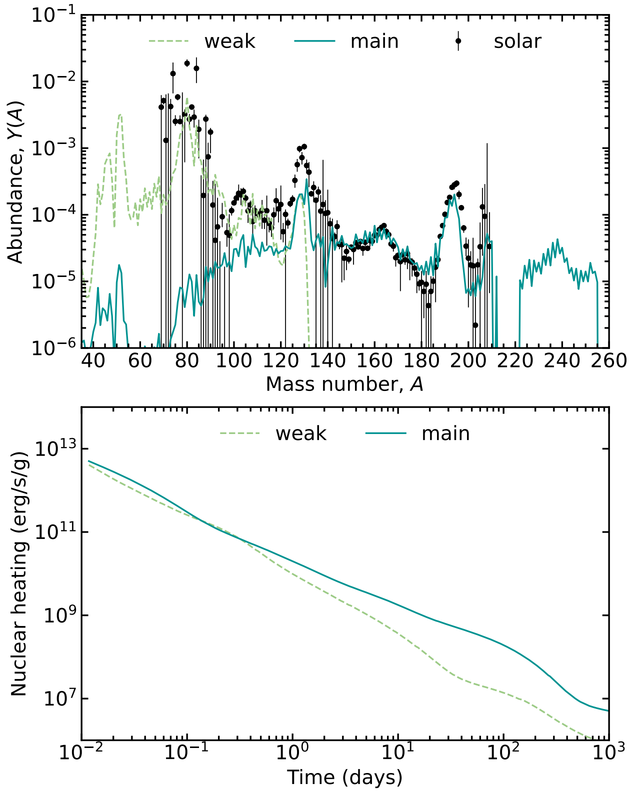

Figure 2. Composition (at one day) and heating in collapsar nucleosynthesis, illustrating both weak and main r-processes.

cretion disk (MacFadyen & Woosley 1999b; Siegel et al. 2019; Miller et al. 2020; Just et al. 2022; Gottlieb et al. 2022; Issa et al. 2025). This long explored mechanism is capable of producing both light and heavy r-process material depending on the treatment of the relevant neutrino physics (Surman et al. 2006). The interaction of matter with high-energy photons represents another avenue for creating neutron-rich conditions associated with the jet (Mumpower et al. 2025). The two sites for nucleosynthesis are shown in Figure 1.

We perform nucleosynthesis calculations with version 1.6.0 of the Portable Routines for Integrated nucleoSynthesis Modeling (PRISM) reaction network (Sprouse et al. 2021). We consider fiducial models for nucleosynthesis from (Mumpower et al. 2025). These models span two possible outcomes: a weak r-process with material up to $A \sim 130$, a complete main r-process that produces second and third peak elements in addition to actinides. The nuclear heating that enters into the kilonova modeling is self-consistently calculated with evolution of abundances as in Zhu et al. (2021). The composition and heating for this work is shown in Figure 2.

2.2. *Kilonova Model*

Our single-component kilonova model consists of a spherically symmetric ejecta component introduced in Wollaeger et al. (2018). The ejecta is taken to be homologously expanding and is parameterized by mass $m_{\rm ej}$ and velocity $v_{\rm ej}$. The spatial discretization consists of 64 radial cells and a maximum grid velocity twice that of $v_{\rm ej}$; Figure 2 in Korobkin et al. (2021) displays the "S" schematic corresponding to this morphology.

We use `SuperNu` (Wollaeger & van Rossum 2014), a Monte Carlo code for simulation of time-dependent radiation transport with matter in local thermodynamic equilibrium, to generate simulated kilonova spectra. The ejecta is assumed to have fixed composition and morphology for the duration of each simulation. The radioactive heating contributions are also weighted by thermalization efficiencies introduced in Barnes et al. (2016) (see Wollaeger et al. (2018) for a detailed description of the adopted nuclear heating). We use detailed opacity calculations via the tabulated, binned opacities generated with the Los Alamos suite of atomic physics codes (Fontes et al. 2015, 2020; Olsen et al. 2023).

The `SuperNu` outputs in this work are post-processed to a source distance of 10 pc, in units of erg s^{-1} cm^{-2} Å^{-1}. The spectra are binned into 1024 equally log-spaced wavelength bins spanning $0.1 \leq \lambda \leq 12.8$ microns. For the purposes of comparison with observations, we convolve our simulated `SuperNu` spectra with the Rubin Observatory *grizy* ($\sim 4000 - 11000$ Å) and 2MASS *JHK* ($\sim 11000 - 24000$ Å) broadband filters to generate broadband light curves in these filters.

2.3. *Fiducial Simulation Grid*

We generate a grid of `SuperNu` simulations characterized by the fiducial ejecta parameters described in Table 1. These fiducial parameters span the same ejecta parameter range as in previous kilonova studies of neutron star mergers (e.g. Coughlin et al. 2018; Wollaeger et al. 2021; Ristić et al. 2022; Gillanders et al. 2023; Ristić et al. 2023; Peng et al. 2024; Desai et al. 2025; Koehn et al. 2025). In comparing directly to the parameters associated with the assumption of a neutron-star-merger kilonova engine, we aim to explore our model's ability to describe the GRB211211A and GRB230307A observations comparably with minimal prior assumptions.

2.4. *Optimized Extension of Fiducial Grid*

We then build upon the grid of fiducial parameter simulations presented in Table 1 and expand our initial library of models to one suitable for surrogate model training. We choose new simulation parameters iteratively by fitting a two-dimensional parabola in [$m_{\rm ej}$, $v_{\rm ej}$]

Ejecta Parameter	Fiducial Values
Mass $m_{\rm ej}$	$0.001, 0.01, 0.1$ $[M_\odot]$
Velocity $v_{\rm ej}$	$0.1, 0.2, 0.3$ $[c]$
r-process Composition	weak, main

Table 1. Fiducial simulation grid ejecta parameters.

space to the log-likelihood ($\ln \mathcal{L}$) associated with each simulation, defined as

$$\ln \mathcal{L} = \sum_{b,t} -\frac{1}{2}\frac{(y_{b,t} - \hat{y}_{b,t})^2}{\sigma^2}, \quad (1)$$

where $y_{b,t}$ corresponds to the observation in a given broadband filter b at time t, $\hat{y}_{b,t}$ the simulation prediction for the same b and t, and σ the observation uncertainty, all in units of AB magnitudes.

We apply the parabolic fit to $\ln \mathcal{L}$ of both GRBs, and iteratively place new simulations in unequally-sized batches based on the fit's prediction of the peak $\ln \mathcal{L}$ for each GRB given the current iteration of the simulation grid. We expand the dynamic range of our parameters during grid refinement, specifically allowing velocities as low as $v_{\rm ej} = 0.01c$ and masses as high as $m_{\rm ej} = 0.5M_\odot$. The final simulation grid consists of 59 total simulations spanning ejecta parameters $10^{-3} \le m_{\rm ej}/M_\odot \le 0.5$ and $0.01 \le v/c \le 0.3$, sufficient for surrogate model training.

Given the success of Gaussian processes (GPs) in similar prior studies (e.g. Coughlin et al. 2018; Ristić et al. 2022), we use the `scikit-learn` (Pedregosa et al. 2011) GP regressor as our surrogate model for this study. We instantiate each GP's hyperparameters as follows: GP length scales are determined by the standard deviation of the inputs ($m_{\rm ej}, v_{\rm ej}$), while the length scale bounds are set by the minima and maxima of the inputs, and our kernel is a product of a `WhiteKernel` and a radial basis function `RBF` kernel. A separate GP is trained for each of the *grizJK* broadband filters considered in this study. Each GP is trained on 54 of the 59 simulations, with five simulations reserved for the test set to ensure fitting fidelity.

For inference, we use the RIFT (Lange et al. 2018) parameter inference algorithm and compare to the observations of each GRB originally reported in Rastinejad et al. (2022) and Yang et al. (2024). Using the adaptive volume sampler in RIFT (Tiwari et al. 2023; Wagner et al. 2025), we optimize over the log-likelihood

$$\ln \mathcal{L} = \sum_{b,t} -\frac{1}{2}\frac{(y_{b,t} - \hat{y}_{b,t})^2}{\sigma^2 + \sigma_{\rm sys}^2}, \quad (2)$$

where all terms are defined as in Equation 1 with the addition of an inference parameter $\sigma_{\rm sys}$ which encapsulates our light-curve fitting systematic uncertainty in units of AB magnitudes. During inference, we scale our `SuperNu` light curves from absolute to apparent AB magnitudes according to the source distances reported in Rastinejad et al. (2022) and Yang et al. (2024), respectively. We terminate our inference analyses upon accruing $\sim 10^3$ effective samples.

3. RESULTS

3.1. *Initial Comparison to Fiducial Light Curves*

We perform an initial comparison of the broadband light curve predictions for our model using fiducial parameters of ejecta outflow (Table 1) to the optical and near-infrared observations associated with GRB 211211A and GRB 23037A, compiled from Rastinejad et al. (2022) and Yang et al. (2024), respectively, with subtracted contribution from the afterglow model. We qualitatively identify that our fiducial model with ejecta outflow parameterized by $m_{\rm ej} = 0.1M_\odot$ and $v_{\rm ej} = 0.2c$ consisting of a weak r-process composition reproduces the light curves of both GRBs. Most notably, prior to any data fitting or fine-tuning of our model parameters, we immediately observe that the $m_{\rm ej} = 0.1M_\odot$, $v_{\rm ej} = 0.2c$ model light curves match *both* the blue and red emission for both GRBs using only a single ejecta component. These ejecta values are consistent with expectations for collapsar ejecta in the literature (Fujimoto et al. 2007; Barnes & Metzger 2023).

3.2. *Parameter Inference with Refined Simulation Grid*

Guided by the fiducial parameter fit, we generate light-curve surrogate models as described in Section 2.4 and recover Bayesian posterior distributions for $m_{\rm ej}$, $v_{\rm ej}$, and $\sigma_{\rm sys}$ for each of the GRBs in this study. Figure 3 presents our best-fit light curves and the associated ejecta and $\sigma_{\rm sys}$ parameters which describe them. As predicted by the naive fiducial light curve fit described earlier, both sets of observations are recovered well by our model's light curves. We find that GRB211211A is well represented by a lighter $m_{\rm ej} = 0.13M_\odot$, fast-moving $v_{\rm ej} = 0.221c$ ejecta, while GRB230307A favors a more massive $m_{\rm ej} = 0.27M_\odot$, slower $v_{\rm ej} = 0.03c$ ejecta, with the latter result corroborated by previous inference of GRB230307A using semi-analytic models (Gillanders et al. 2023). We note that the velocity posteriors for GRB230307A do exhibit weak support for a fast-moving ejecta comparable to that of GRB211211A. In our study, we also examine the light curves associated with an intermediate and full r-process, but find that these com-

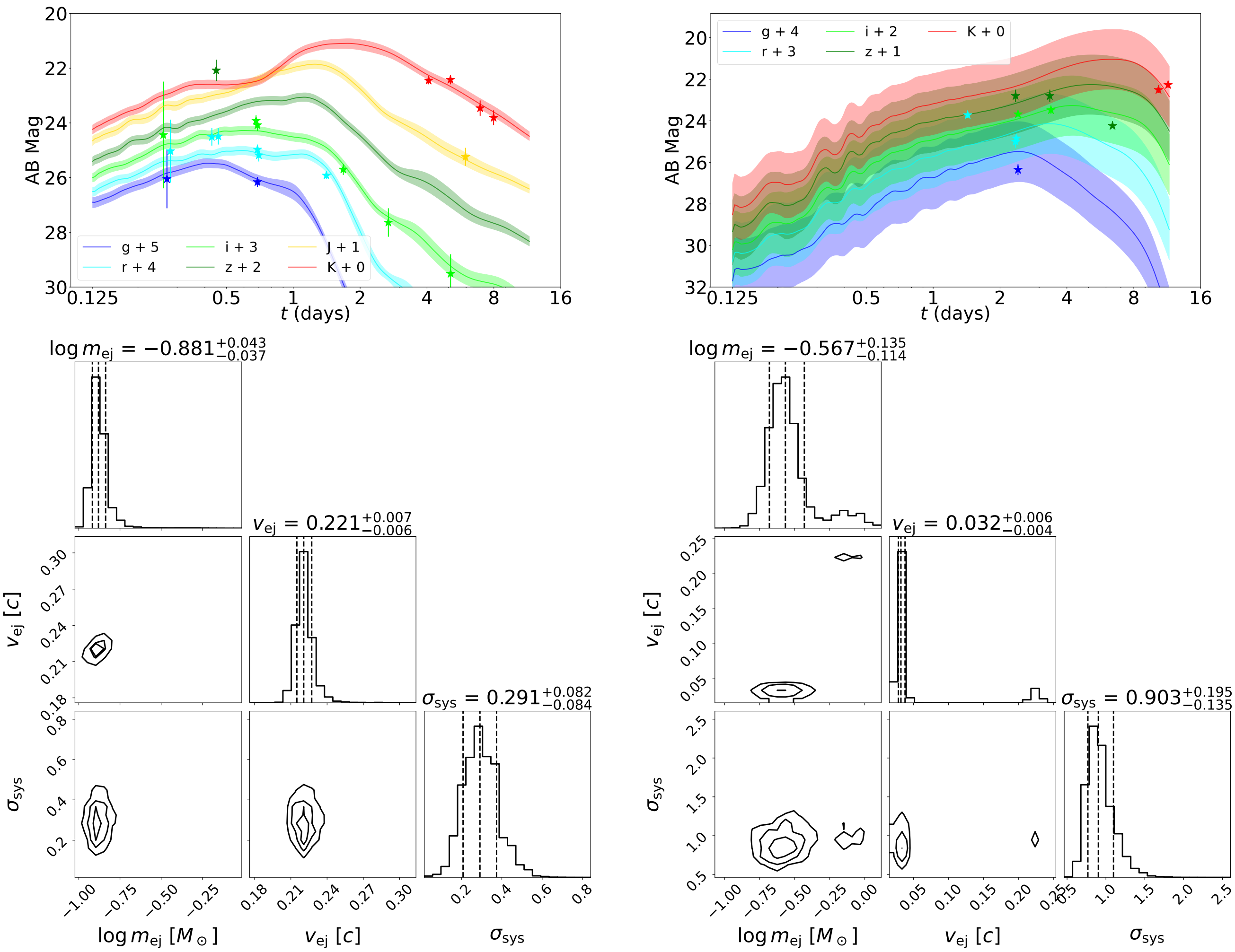

Figure 3. GRB 211211A (left) and GRB 230307A (right) optical/near-infrared observations compared to the best-fit interpolated light curve characterized by the parameter values reported in the posterior plots under the assumption of a weak r-process ejecta composition. The r and i observations at 0.27 days are artificially separated by ± 0.01 days for visual clarity.

positions are unable to recover the blue emission successfully regardless of ejecta kinematic parameters.

4. DISCUSSION

The relatively large ejecta masses favored in our fits are, in principle, also possible in a scenario in which nucleosynthesis is occurring in the disk of the collapsar (e.g. Siegel et al. 2019). However, the high velocities (GRB211211A) and sharply-peaked velocity posteriors (GRB230307A) predicted in our inference disfavor this scenario, as disk winds are typically slower-peaked with long tails (Miller et al. 2020). Moreover, these ejecta masses rule out double neutron star mergers as the source of the nucleosynthesis, and are at the very edge of what is reasonably possible for a black hole-neutron star merger progenitor (Fernández et al. 2017; Curtis et al. 2023).

In Section 3.2, we identify that our model is capable of matching the blue and red emission simultaneously using a single ejecta component. This match is in contrast to neutron-star-merger kilonovae, which require at least two separate ejecta components with appreciably different parameterizations to successfully fit both early-time blue and late-time red emission (see e.g., Cowperthwaite et al. 2017; Evans et al. 2017; Kasliwal et al. 2017; Smartt et al. 2017; Tanvir et al. 2017; Troja et al. 2017; Villar et al. 2017). Moreover, for GRB 211211A, Hamidani et al. (2024) could not find a good fit even with a two-component kilonova model, and proposed a scenario where the emission is additionally powered by a late central engine activity. The blue emission in our model arises from the weak r-process composition producing lighter elements than the lanthanides, resulting in a low opacity ejecta which permits the propagation of higher energy, blue photons; the lack of lanthanides does not impede late-time infrared emission since the ejecta mass is sufficiently high compared to neutron star merger ejecta to allow for the emission of infrared thermal photons. Similarly, the presence of a near-infrared emission "bump" (that exceeds the fading afterglow flux in this energy band) has previously been used as evidence of the production of lanthanides, indicating the presence of r-process nucleosynthesis (e.g. Gillanders et al. 2023). Recent studies, however, have shown that late-time infrared emission can occur even without the r-process. For example, Tak et al. (2023) and Fryer et al. (2024) found that different assumptions for the ejecta velocity distribution can yield late-time features in the light curves which can mimic those typically associated with heavy-element production. Building upon the hypothesis of a white-dwarf neutron-star (WDNS) merger as the GRB211211A progenitor (Yang et al. 2022), Liu et al. (2025) find that a WDNS merger produces nucleosynthetic yields encompassing only a fraction of the first r-process peak with no heavy element nucleosynthesis. These scenarios add to the growing body of evidence against the contemporary viewpoint that a red kilonova is a "smoking gun" of lanthanide production.

In their respective analyses, both Rastinejad et al. (2022) and Yang et al. (2024) infer ejecta properties using semi-analytic prescriptions which do not account for microphysical details such as photon reprocessing and radiative heating. Inference using models without these microphysical details can lead to, among other things, overestimation of ejecta mass to compensate for the missing radiative heating contribution. Our study encompasses these important effects and nevertheless recovers large ejecta masses, lending further confidence to our analysis favoring a collapsar nucleosynthesis scenario over one involving a merger. Our study is partially motivated by the importance of including photon reprocessing and radiative heating microphysical effects when studying transients and understanding their discriminatory value in identifying transient progenitor candidates. Such details can have significant downstream consequences, such as when inferring GRB progenitor populations and their effects on galactic chemical evolution (Rastinejad et al. 2025).

In Section 3.2, we specify that the GRB230307A posteriors exhibit weak support for a high-velocity ejecta component. In our fiducial simulation library, a comparison of weak r-process simulations with fixed $m_{\rm ej} = 0.1 M_\odot$ for $v_{\rm ej}/c = [0.05, 0.07, 0.10, 0.15, 0.18, 0.20, 0.30]$ finds greater variation across all broadband filters at early times ($t < 1$ day) compared to late times ($t > 1$ day). This greater variation establishes that earlier observations carry more discriminating power for ejecta velocity; the relatively late-time ($t \gtrsim 1.5$ days) observations of GRB230307A thus set an upper limit on our ability to constrain the ejecta velocity, as evidenced by the weakly-supported high-velocity posterior. We also recover significantly larger systematic uncertainty in our inference of GRB230307A, again owing largely to the limited dataset which lacks early-time observations and thus inhibits constraint on the full evolution of the light curves. Our GRB230307A inference results highlight the community's need for established plans for rapid kilonova and gravitational-wave counterpart follow-up observations (Magee et al. 2021; Burns et al. 2025; Desai et al. 2025; Plestkova et al. 2025; Singer et al. 2025).

5. CONCLUSION

Our work provides strong support for the idea that collapsars are a viable origin for the kilonovae associated with long-duration gamma-ray bursts. We have demonstrated that the composition of weak r-process elements (up to proton number $Z \sim 50$ or mass number $A \sim 130$) can produce a spectrally evolving red component in kilonova emission. Thus a red kilonova does not inherently imply the synthesis of heavy r-process material — a view that challenges contemporary interpretations. These insights prompt a reassessment of kilonova modeling assumptions and the inferred nucleosynthetic yields from such events. Future multi-messenger observations that include gravitational wave detections will be critical in distinguishing between the proposed mechanisms responsible for kilonovae associated with long-duration gamma-ray bursts.

6. ACKNOWLEDGMENTS

Los Alamos National Laboratory (LANL) is operated by Triad National Security, LLC, for the National Nuclear Security Administration of U.S. Department of Energy (Contract No. 89233218CNA000001). M. R. acknowledges support from the Information Science & Technology Institute (ISTI) at LANL as an ISTI Postdoctoral Fellow and acknowledges PECASE award funds. B. L. B. acknowledges support from the Advanced Simulation and Computing Program of LANL as a Metropolis Postdoc Fellow. N.L.-R. acknowledges support from the Laboratory Directed Research and Development program of LANL project numbers 20230115ER and 20230217ER. O. K. is supported by the Laboratory Directed Research project 20240170ER. S. C., A .G. and M. R. M. acknowledge support from the Laboratory Directed Research and Development program of LANL project numbers 20230052ER and 20240004DR. This research used resources provided by LANL through the

Institutional Computing program. This document has been assigned LA-UR-25-28887.

REFERENCES

Barnes, J., Kasen, D., Wu, M.-R., & Martínez-Pinedo, G. 2016, The Astrophysical Journal, 829, 110, doi: 10.3847/0004-637X/829/2/110

Barnes, J., & Metzger, B. D. 2023, ApJ, 947, 55, doi: 10.3847/1538-4357/acc384

Blandford, R. D., & Znajek, R. L. 1977, MNRAS, 179, 433, doi: 10.1093/mnras/179.3.433

Bloom, J. S., Kulkarni, S. R., & Djorgovski, S. G. 2002, AJ, 123, 1111, doi: 10.1086/338893

Bromberg, O., Granot, J., Lyubarsky, Y., & Piran, T. 2014, MNRAS, 443, 1532, doi: 10.1093/mnras/stu995

Bromberg, O., Nakar, E., Piran, T., & Sari, R. 2011, ApJ, 740, 100, doi: 10.1088/0004-637X/740/2/100

—. 2012, ApJ, 749, 110, doi: 10.1088/0004-637X/749/2/110

Burns, E., Fryer, C. L., Agullo, I., et al. 2025, arXiv e-prints, arXiv:2502.03577, doi: 10.48550/arXiv.2502.03577

Côté, B., Eichler, M., Arcones, A., et al. 2019, ApJ, 875, 106, doi: 10.3847/1538-4357/ab10db

Coughlin, M. W., Dietrich, T., Doctor, Z., et al. 2018, MNRAS, 480, 3871, doi: 10.1093/mnras/sty2174

Cowperthwaite, P. S., Berger, E., Villar, V. A., et al. 2017, ApJL, 848, L17, doi: 10.3847/2041-8213/aa8fc7

Curtis, S., Miller, J. M., Fröhlich, C., et al. 2023, The Astrophysical Journal Letters, 945, L13, doi: 10.3847/2041-8213/acba16

Desai, M. M., Chatterjee, D., Jhawar, S., et al. 2025, MNRAS, 541, 2619, doi: 10.1093/mnras/staf1045

Evans, P. A., Cenko, S. B., Kennea, J. A., et al. 2017, Science, 358, 1565, doi: 10.1126/science.aap9580

Fernández, R., Foucart, F., Kasen, D., et al. 2017, Classical and Quantum Gravity, 34, 154001, doi: 10.1088/1361-6382/aa7a77

Fong, W., & Berger, E. 2013, ApJ, 776, 18, doi: 10.1088/0004-637X/776/1/18

Fong, W., Berger, E., & Fox, D. B. 2010, ApJ, 708, 9, doi: 10.1088/0004-637X/708/1/9

Fontes, C. J., Fryer, C. L., Hungerford, A. L., Wollaeger, R. T., & Korobkin, O. 2020, MNRAS, 493, 4143, doi: 10.1093/mnras/staa485

Fontes, C. J., Zhang, H. L., Abdallah Jr., J., et al. 2015, Journal of Physics B Atomic Molecular Physics, 48, 144014, doi: 10.1088/0953-4075/48/14/144014

Fryer, C. L., Hungerford, A. L., Wollaeger, R. T., et al. 2024, ApJ, 961, 9, doi: 10.3847/1538-4357/ad1036

Fujimoto, S.-i., Hashimoto, M.-a., Kotake, K., & Yamada, S. 2007, ApJ, 656, 382, doi: 10.1086/509908

Galama, T. J., Vreeswijk, P. M., van Paradijs, J., et al. 1998, Nature, 395, 670, doi: 10.1038/27150

Ghirlanda, G., Nappo, F., Ghisellini, G., et al. 2018, A&A, 609, A112, doi: 10.1051/0004-6361/201731598

Gillanders, J. H., Troja, E., Fryer, C. L., et al. 2023, arXiv e-prints, arXiv:2308.00633, doi: 10.48550/arXiv.2308.00633

Gottlieb, O., Lalakos, A., Bromberg, O., Liska, M., & Tchekhovskoy, A. 2022, MNRAS, 510, 4962, doi: 10.1093/mnras/stab3784

Gottlieb, O., Metzger, B. D., Foucart, F., & Ramirez-Ruiz, E. 2025, ApJ, 984, 77, doi: 10.3847/1538-4357/adc577

Hamidani, H., Tanaka, M., Kimura, S. S., Lamb, G. P., & Kawaguchi, K. 2024, ApJL, 971, L30, doi: 10.3847/2041-8213/ad6864

Hjorth, J., & Bloom, J. S. 2012, Gamma-ray bursts

Hjorth, J., Sollerman, J., Møller, P., et al. 2003, Nature, 423, 847, doi: 10.1038/nature01750

Issa, D., Gottlieb, O., Metzger, B. D., et al. 2025, ApJL, 985, L26, doi: 10.3847/2041-8213/adc694

Just, O., Aloy, M. A., Obergaulinger, M., & Nagataki, S. 2022, ApJL, 934, L30, doi: 10.3847/2041-8213/ac83a1

Kasliwal, M. M., Nakar, E., Singer, L. P., et al. 2017, Science, 358, 1559, doi: 10.1126/science.aap9455

Koehn, H., Wouters, T., Pang, P. T. H., et al. 2025, arXiv e-prints, arXiv:2507.13807, doi: 10.48550/arXiv.2507.13807

Korobkin, O., Wollaeger, R. T., Fryer, C. L., et al. 2021, ApJ, 910, 116, doi: 10.3847/1538-4357/abe1b5

Kouveliotou, C., Meegan, C. A., Fishman, G. J., et al. 1993, ApJL, 413, L101, doi: 10.1086/186969

Lange, J., O'Shaughnessy, R., & Rizzo, M. 2018, arXiv e-prints, arXiv:1805.10457, doi: 10.48550/arXiv.1805.10457

Levan, A. J., Gompertz, B. P., Salafia, O. S., et al. 2024, Nature, 626, 737, doi: 10.1038/s41586-023-06759-1

Liu, X.-X., Lü, H.-J., Chen, Q.-H., Du, Z.-W., & Liang, E.-W. 2025, ApJL, 988, L46, doi: 10.3847/2041-8213/adec83

Lyman, J. D., Levan, A. J., Tanvir, N. R., et al. 2017, MNRAS, 467, 1795, doi: 10.1093/mnras/stx220

MacDonald, D., & Thorne, K. S. 1982, MNRAS, 198, 345, doi: 10.1093/mnras/198.2.345

MacFadyen, A. I., & Woosley, S. E. 1999a, ApJ, 524, 262, doi: 10.1086/307790
—. 1999b, ApJ, 524, 262, doi: 10.1086/307790
Magee, R., Chatterjee, D., Singer, L. P., et al. 2021, ApJL, 910, L21, doi: 10.3847/2041-8213/abed54
Miller, J. M., Sprouse, T. M., Fryer, C. L., et al. 2020, ApJ, 902, 66, doi: 10.3847/1538-4357/abb4e3
Mumpower, M. R., Lee, T.-S. H., Lloyd-Ronning, N., et al. 2025, ApJ, 982, 81, doi: 10.3847/1538-4357/adb1e3
Negro, M., Cibrario, N., Burns, E., et al. 2025, ApJ, 981, 14, doi: 10.3847/1538-4357/ada8a9
Olsen, K., Fontes, C. J., Fryer, C. L., et al. 2023, NIST-LANL Lanthanide Opacity Database (ver. 1.2), [Online]. Available: https://nlte.nist.gov/OPAC [Apr 11 2023], doi: 10.18434/mds2-2375
Pedregosa, F., Varoquaux, G., Gramfort, A., et al. 2011, Journal of Machine Learning Research, 12, 2825
Peng, Y., Ristić, M., Kedia, A., et al. 2024, Physical Review Research, 6, 033078, doi: 10.1103/PhysRevResearch.6.033078
Plestkova, N., Sravan, N., Weizmann Kiendrebeogo, R., et al. 2025, arXiv e-prints, arXiv:2507.11785, doi: 10.48550/arXiv.2507.11785
Ramirez-Ruiz, E., Celotti, A., & Rees, M. J. 2002, MNRAS, 337, 1349, doi: 10.1046/j.1365-8711.2002.05995.x
Rastinejad, J. C., Fong, W., Kilpatrick, C. D., Nicholl, M., & Metzger, B. D. 2025, ApJ, 979, 190, doi: 10.3847/1538-4357/ad9c77
Rastinejad, J. C., Gompertz, B. P., Levan, A. J., et al. 2022, Nature, 612, 223, doi: 10.1038/s41586-022-05390-w
Ristić, M., O'Shaughnessy, R., Villar, V. A., et al. 2023, Physical Review Research, 5, 043106, doi: 10.1103/PhysRevResearch.5.043106
Ristić, M., Champion, E., O'Shaughnessy, R., et al. 2022, Physical Review Research, 4, 013046, doi: 10.1103/PhysRevResearch.4.013046
Saleem, M., Chen, H.-Y., Siegel, D. M., et al. 2025, arXiv e-prints, arXiv:2508.06020. https://arxiv.org/abs/2508.06020
Siegel, D. M., Barnes, J., & Metzger, B. D. 2019, Nature, 569, 241, doi: 10.1038/s41586-019-1136-0
Singer, L. P., Criswell, A. W., Leggio, S. C., et al. 2025, PASP, 137, 074501, doi: 10.1088/1538-3873/adcfc6
Smartt, S. J., Chen, T. W., Jerkstrand, A., et al. 2017, Nature, 551, 75, doi: 10.1038/nature24303
Sprouse, T. M., Mumpower, M. R., & Surman, R. 2021, PhRvC, 104, 015803, doi: 10.1103/PhysRevC.104.015803
Sun, H., Wang, C. W., Yang, J., et al. 2025, National Science Review, 12, nwae401, doi: 10.1093/nsr/nwae401
Surman, R., McLaughlin, G. C., & Hix, W. R. 2006, ApJ, 643, 1057, doi: 10.1086/501116
Tak, D., Uhm, Z. L., & Gillanders, J. H. 2023, ApJ, 958, 121, doi: 10.3847/1538-4357/ad06b0
Tanvir, N. R., Levan, A. J., González-Fernández, C., et al. 2017, The Astrophysical Journal, 848, L27, doi: 10.3847/2041-8213/aa90b6
The LIGO Scientific Collaboration, the Virgo Collaboration, Abbott, B. P., et al. 2017a, PhRvL, 119, 161101, doi: 10.1103/PhysRevLett.119.161101
—. 2017b, ApJL, 848, L13, doi: 10.3847/2041-8213/aa920c
Tiwari, V., Hoy, C., Fairhurst, S., & MacLeod, D. 2023, PhRvD, 108, 023001, doi: 10.1103/PhysRevD.108.023001
Troja, E., Piro, L., van Eerten, H., et al. 2017, Nature, 551, 71, doi: 10.1038/nature24290
Troja, E., Fryer, C. L., O'Connor, B., et al. 2022, Nature, 612, 228, doi: 10.1038/s41586-022-05327-3
Villar, V. A., Guillochon, J., Berger, E., et al. 2017, ApJL, 851, L21, doi: 10.3847/2041-8213/aa9c84
Wagner, K. J., O'Shaughnessy, R., Yelikar, A., et al. 2025, arXiv e-prints, arXiv:2505.11655, doi: 10.48550/arXiv.2505.11655
Wollaeger, R. T., & van Rossum, D. R. 2014, The Astrophysical Journal Supplement Series, 214, 28, doi: 10.1088/0067-0049/214/2/28
Wollaeger, R. T., Korobkin, O., Fontes, C. J., et al. 2018, Monthly Notices of the Royal Astronomical Society, 478, 3298, doi: 10.1093/mnras/sty1018
Wollaeger, R. T., Fryer, C. L., Chase, E. A., et al. 2021, The Astrophysical Journal, 918, 10, doi: 10.3847/1538-4357/ac0d03
Woosley, S., & Bloom, J. 2006, Annu. Rev. Astron. Astrophys., 44, 507
Woosley, S. E. 1993, ApJ, 405, 273, doi: 10.1086/172359
Yang, J., Ai, S., Zhang, B.-B., et al. 2022, Nature, 612, 232, doi: 10.1038/s41586-022-05403-8
Yang, Y.-H., Troja, E., O'Connor, B., et al. 2024, Nature, 626, 742, doi: 10.1038/s41586-023-06979-5
Zhang, H.-M., Huang, Y.-Y., Zheng, J.-H., Liu, R.-Y., & Wang, X.-Y. 2022, ApJL, 933, L22, doi: 10.3847/2041-8213/ac7b23
Zhu, Y. L., Lund, K. A., Barnes, J., et al. 2021, ApJ, 906, 94, doi: 10.3847/1538-4357/abc69e